

# Topology Optimization of Freeform Shells by Employing Isogeometric Analysis

Hossein Ghasemnejad<sup>1\*</sup>, Seyed Mehdi Tavakkoli<sup>2</sup>, Behrooz Hassani<sup>3</sup>

<sup>1</sup> Department of Civil Engineering, Ayatollah Amoli branch, Islamic Azad University, P.O.B. 678, 4615143358 Amol, Iran

<sup>2</sup> Department of Civil Engineering, Shahrood University of Technology, P.O.B. 316, 3619995161 Shahrood, Iran

<sup>3</sup> Department of Mechanical Engineering, Ferdowsi University of Mashhad, 9177948974 Mashhad, Iran

\* Corresponding author, e-mail: [Hossein.ghasemnejad@yahoo.com](mailto:Hossein.ghasemnejad@yahoo.com)

Received: 09 July 2024, Accepted: 11 November 2024, Published online: 22 November 2024

## Abstract

Topology optimization has attracted significant attention for creating efficient structures in shells. One of the prominent methods in the field is the Solid Isotropic Materials with Penalization (SIMP) approach which is typically employed alongside finite element method (FEM). However in classical FEM, achieving a smooth shell surface, necessitates a considerable number of elements, leading to high computational cost. In this article an Isogeometric Analysis (IGA) based technique is utilized to determine the optimum topology of freeform shell structures. The proposed approach follows the methodology of SIMP by defining a density function over a design domain to parametrize the optimization problem so that zero value represents void areas and one denotes solid parts. Non-Uniform Rational B-splines (NURBS) are employed for structural analysis as well as for interpolating density function for topology optimization (TO). Two models are employed: one with coarse mesh for defining the geometry and another with a fine mesh for analysis and optimization. The Method of Moving Asymptotes (MMA) is employed to solve the optimization problem. A few examples are presented, and the results are discussed and compared with literature in one case to verify the proposed method. It is demonstrated that the proposed approach is efficient in finding the optimum topology of shell structures. The findings show that finer control nets results in clearer boundaries. It was observed that the penalty exponent is essential for obtaining an acceptable solution. It was also noted that the influence of the NURBS degree on optimal topology is trivial.

## Keywords

topology optimization, freeform shell, Isogeometric analysis, SIMP

## 1 Introduction

Structural optimization (SO) has received significant attention in recent decades. Finding the best possible structure for bearing the applied loads and satisfaction of design demands is the purpose of SO. Optimization of structures can be carried out in three stages. TO is the first stage, where the configuration of the structure is determined. In the next stage, the optimum shape of structure is sought. During this process, the topology remains fixed while the boundaries of the structure are modified to reach an optimal position. Finally, in size optimization, the geometric properties of the members, such as cross section, are optimized. This paper focuses on topology optimization of freeform shell structures.

TO was first introduced by Maxwell [1] and since then it has been applied in a wide range of structural fields, including truss structures [2–5], skeletal structures [6–8],

shear walls [9, 10] and shells [11–13] over the past few decades. Some other new works of TO can be reviewed in [14–16]. For a comprehensive review [17].

Bendsøe and Kikuchi [18] introduced the homogenization approach for TO. In this method, the geometric properties of micro scale holes are optimized and homogenization bridges micro and macro structures to obtain mechanical properties of macro structure. To simplify the parameterization, the SIMP method is introduced by Bendsøe [19] where a density function, restricted to values between zero (for voids) and one (for solid), is distributed in design domain to determine the topology of the structure. A penalty exponent is implemented to prevent the formation of regions with intermediate densities which are not desirable in practice. This method has been used in many researches in finite element based topology optimization [20].

Since the introduction of the IGA method [21], it has been widely used in structural analysis research. This method is a logical generalization of the classical finite element method (FEM), inspired by computer aided geometric design (CAGD). In this approach, NURBS basis functions are employed to approximate the unknown function to find their values at control points. The IGA has also been utilized in topology optimization. Isogeometric topology optimization (ITO) can be classified into three general categories [22]: density-based [23–25], level set-based [26–28] and moving morphable components/voids (MMC/V)-based [29–31] methods. The method used in this article belongs to the density-based methods.

Due to their low weight and high efficiency, shell structures are highly regarded by structural designers. Meanwhile, freeform shell structures are important due to their favorable performance and high flexibility in producing desired shapes. Obviously, finding the optimal shape and layout of this type of structures is of particular importance. Many studies have focused on finding the optimal shape of shells, but research on the optimization of shell topology has been relatively limited. One of the early works in this field was conducted by Maute and Ramm [11]. Other studies in the literature can be found in [32–34]. Clausen et al. [35] presented the topology optimization of shell with porous infill. Townsend and Kim [36] introduced a method that uses level set principles to find the optimal topology of shells. The integrated optimization of shape and topology is another area of research in shell optimization. Ansola et al [37–39] presented the combined optimization of shells in which the shape and topology optimization steps are performed sequentially. The authors of the present article investigated the simultaneous optimization of shape and topology, where both variables of shape and topology, are parameterized and optimized simultaneously [12]. Recently, a research has been carried out that considers the shape, topology, and thickness components simultaneously in the optimization procedure [40].

In all studies reviewed in this section, the parameterization of the SIMP based shell topology problem is grounded on FEM which has limitations in computational accuracy. Achieving high accuracy with FEM requires a large number of elements, leading to significant computational demands. Additionally, in the classic FEM, the geometric and analytical parameters are different which results in parametrical complexities. To address these limitations, this paper introduces an Isogeometric Analysis -based SIMP method for optimizing the topology of shell structures.

In the current research, the process of generating geometry of the mid-surface of shells, analysis and TO parameterization are all carried out using IGA basics and hence it can be said that it is much more straightforward than other reviewed methods based on finite elements. Furthermore, employing isogeometric as the analysis tool removes the necessity for mesh generation. This issue simplifies computational complexity which is crucial in terms of calculations costs. The presented method uses the basics of SIMP and distribution of materials in the design domain is carried out using NURBS functions. The values of this function at control points are considered as design variables in the optimization problem and its optimal distribution on the design domain is found.

The outline of this paper is as follows. In Section 2, the NURBS basics and IGA for shell structures are explained. TO is described in Section 3. In Sections 4, the optimization procedure of this article is presented. Sensitivity analysis, which is a requirement for optimization by mathematical methods, is discussed in Section 5. In Section 6, numerical examples will be presented and the results will be discussed. Finally, the article ends with the conclusion in Section 7.

## 2 NURBS basics and IGA for shells

IGA is a computational approach that integrates CAGD and computer aided engineering (CAE) in a unified framework. In this approach, following the principles of standard FEM, both geometry and displacement components are approximated using NURBS basis functions instead of standard polynomial functions.

### 2.1 Summary of NURBS fundamentals

To explain NURBS, one needs to introduce B-spline basis functions. The  $i$ -th B-spline basis function of degree  $p$  denoted by  $N_{i,p}(r)$  is defined recursively as:

$$N_{i,0}(r) = \begin{cases} 1 & \text{if } r_i \leq r \leq r_{i+1} \\ 0 & \text{otherwise} \end{cases}$$

$$N_{i,p}(r) = \frac{r - r_i}{r_{i+p} - r_i} N_{i,p-1}(r) + \frac{r_{i+p+1} - r}{r_{i+p+1} - r_{i+1}} N_{i+1,p-1}(r) \quad (1)$$

Where  $r = \{r_0, r_1, \dots, r_{m_r}\}$  is the knot vector and  $r_i$  are non-decreasing sequence of real numbers which are called knots. Knots define the parametric space of curves and surfaces

in NURBS methodology. A knot vector is called open if the first and last knots have the multiplicity of  $p + 1$ . In this case the number of knots is equal to  $m = n + p + 1$ . By introducing a positive weight  $W_i$  to B-spline basis functions, a NURBS basis function is defined as:

$$R_{i,p}(r) = \frac{N_{i,p}(r)w_i}{\sum_{j=0}^n N_{j,p}(r)w_j} \quad (2)$$

Also, four important properties of NURBS basis functions are briefly described as follows: (1) Nonnegativity:  $R_{i,p}(r) \geq 0$ ; (2) Local support:  $R_{i,p}(r) = 0$  for  $i \notin [r_i, r_{i+p+1}]$ ; (3) Partition of unity:  $\sum_{i=0}^n R_{i,p}(r) = 1$  and (4) Continuity:  $C^{p-m}$ .

Two dimensional NURBS basis function of order  $p$  and  $q$  in  $r$  and  $s$  directions respectively, can be constructed as:

$$R_{i,j}^{p,q}(r,s) = \frac{N_{i,p}(r)N_{j,q}(s)w_{ij}}{\sum_{k=0}^{n_p} \sum_{l=0}^{n_q} N_{k,p}(r)N_{l,q}(s)w_{kl}} \quad (3)$$

where  $N_{j,q}(s)$  is the B-spline basis function of degree  $q$  in other parametric direction  $s$ , constructed by its knot vector  $s = \{s_0, s_1, \dots, s_{m_q}\}$ . Then a NURBS surface can be defined as:

$$\mathbf{S}(r,s) = \sum_{i=0}^{n_p} \sum_{j=0}^{n_q} R_{i,j}^{p,q}(r,s) \mathbf{P}_{ij} \quad (4)$$

where  $\mathbf{P}_{ij}$  are a set of  $n_p \times n_q$  control points.

## 2.2 IGA for shell structures

In this section, the IGA model for shell structures is described. This model is constructed by borrowing the idea of curved elements [41] for ordinary FEM of shells, and developing it for the IGA, by using NURBS. In this model, assumptions of Reissner Mindlin theory [42] for analysis of thick shells are used. For this purpose, rotational degrees of freedom should be included independently in the analytical model. For a typical shell shown in Fig. 1, by using NURBS basis functions, and defining the coordinate axis  $t$  which is perpendicular to the surface of the shell and varies between  $-1$  and  $1$ , the geometry can be defined in Cartesian coordinate system as follows:

$$\mathbf{X} = \sum_{i=0}^{n_p} \sum_{j=0}^{n_q} R_{i,j}^{p,q}(r,s) \left( \mathbf{P}_{ij} + \frac{1}{2} t T_{ij} \mathbf{V}_{3ij} \right) \quad (5)$$

where  $T_{ij}$  stands for the thickness of the shell in each control point and  $\mathbf{V}_{3ij}$  is the corresponding unit vector in the direction normal to the mid-surface of the shell. The displacement vector of any arbitrary point on the shell surface can be obtained as:

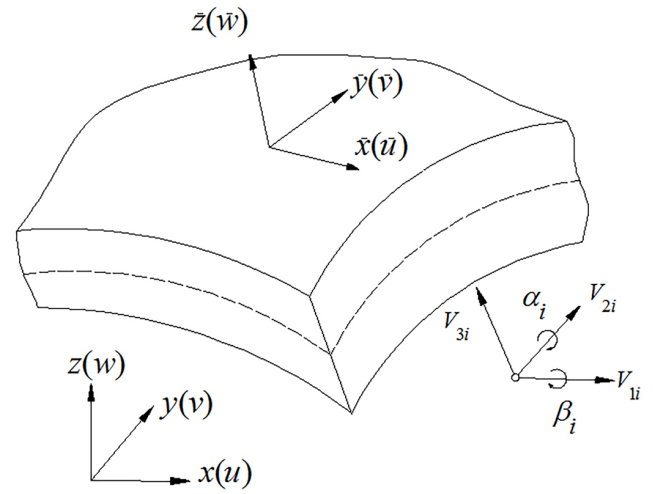


Fig. 1 Shell element, normal vectors, rotational degrees of freedom and global and local coordinate systems

$$\mathbf{U} = \sum_{i=0}^{n_p} \sum_{j=0}^{n_q} R_{i,j}^{p,q}(r,s) \left( \mathbf{U}_{ij} + \frac{1}{2} t T_{ij} [\mathbf{V}_{1ij} - \mathbf{V}_{2ij}] \begin{Bmatrix} \alpha_{ij} \\ \beta_{ij} \end{Bmatrix} \right) \quad (6)$$

$\mathbf{V}_{1ij}$  and  $\mathbf{V}_{2ij}$  are two orthogonal unit vectors normal to  $\mathbf{V}_{3ij}$ .  $\mathbf{U}_{ij}$  is the displacement vector corresponding to the control point  $ij$  where  $\alpha_{ij}$  and  $\beta_{ij}$  are the rotations about  $\mathbf{V}_{1ij}$  and  $\mathbf{V}_{2ij}$ , respectively. It should be noted that the control net is not necessarily placed on the surface of the shell, and as a result, the definition of unit vectors seems ambiguous. To solve this problem, a mapping pattern should be defined that links each control point to a point in the physical space [43]. In this case, rotations can be assigned to these points. Therefore, the translational degrees of freedom are assigned to the control points and the rotational ones are assigned to the points corresponding to each of them on the mid-surface of the shell (Fig. 2).

In order to form shell formulation, local coordinates system is defined at every point of the shell mid-surface. In this system, one of the coordinate axes is perpendicular to the surface of the shell, and the directions of the other two orthogonal axes can be chosen arbitrarily. It should be noted that these two axes should be selected in such a way that the displacement boundary conditions of the problem are easily modeled. In this article, Eqs. (7–8) are used to construct unit vectors  $\mathbf{V}_1$  and  $\mathbf{V}_2$  to find the directions of 1 and 2, respectively.

$$\mathbf{V}_1 = \frac{[x_{,r} \ y_{,r} \ z_{,r}]^T}{(x_{,r}^2 + y_{,r}^2 + z_{,r}^2)^{0.5}} \quad (7)$$

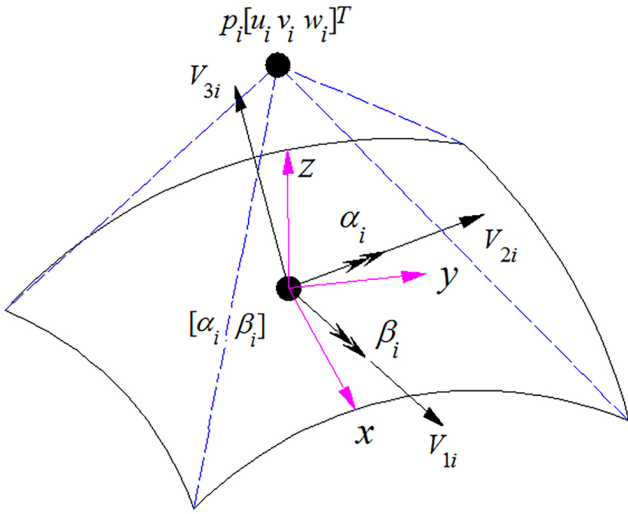


Fig. 2 Translational degrees of freedom at the control point and rotational degrees of freedom at the corresponding point in the mid-surface of the shell

$$V_2 = \frac{[x_{,s} \ y_{,s} \ z_{,s}]^T}{(x_{,s}^2 + y_{,s}^2 + z_{,s}^2)^{0.5}} \quad (8)$$

Vector  $V_3$  which shows the third direction can be obtained from the cross product of the two vectors  $V_1$  and  $V_2$  according to Eq. (9):

$$V_3 = V_1 \times V_2 \quad (9)$$

The three unit vectors introduced here represent directions of local axes at each arbitrary point. With these local axes, the necessary parameters are converted from the global coordinate system to the local one, Finally, the virtual work relationship for an element is expressed in local coordinates and the stiffness matrix is obtained. If the strain vector in the local system is expressed by  $\bar{\epsilon}$ , according to the standard finite element formulation, it can be written as:

$$\bar{\epsilon} = \bar{B}a \quad (10)$$

where  $a$  is the vector of control point's displacements and  $\bar{B}$  is strain displacement matrix. In this case, the stiffness matrix is obtained from:

$$k = \int \bar{B}^T \bar{N} \bar{B} \, dx dy dz \quad (11)$$

where  $\bar{D}$  is the shell elasticity matrix in local coordinate system, which is equal to elasticity matrix of isotropic material. Finally, if the Gaussian integration method is used, the stiffness matrix can be obtained by performing the following transformations. The first transformation is from the physical space to the parametric space (NURBS), which is carried out by:

$$dx dy dz = \det J_1 dr ds dt \quad (12)$$

where Jacobian matrix  $J_1$  is defined as:

$$J_1 = \begin{bmatrix} x_{,r} & y_{,r} & z_{,r} \\ x_{,s} & y_{,s} & z_{,s} \\ x_{,t} & y_{,t} & z_{,t} \end{bmatrix} \quad (13)$$

And the second transformation, from parametric space to Gauss space, is performed according to:

$$\det J_1 dr ds dt = \det J_1 \det J_2 d\xi d\eta d\zeta \quad (14)$$

where  $\xi$ ,  $\eta$  and  $\zeta$  are Gauss integration parameters which are defined in the interval  $[-1,1]$ . The relationship between parameter space and Gauss space can be expressed by:

$$r = \frac{1}{2} [(r_{i+1} - r_i)\xi + (r_{i+1} + r_i)] \quad (15)$$

$$s = \frac{1}{2} [(s_{i+1} - s_i)\eta + (s_{i+1} + s_i)] \quad (16)$$

$$t = \zeta \quad (17)$$

The second Jacobian matrix  $J_2$ , is expressed as:

$$J_2 = \begin{bmatrix} r_{,\xi} & s_{,\xi} & t_{,\xi} \\ r_{,\eta} & s_{,\eta} & t_{,\eta} \\ r_{,\zeta} & s_{,\zeta} & t_{,\zeta} \end{bmatrix} \quad (18)$$

The members of this matrix can be obtained by differentiating Eqs. (1–17). Fig. 3 shows the schematic illustration of physical, parametric and Gauss spaces and the relations between them.

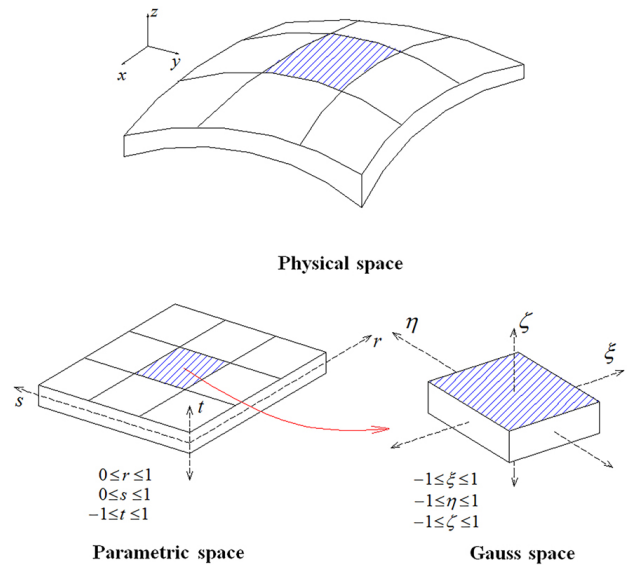


Fig. 3 Schematic illustration of physical, parametric and Gauss spaces

### 3 Topology optimization

One of the primary methods in the development of TO is homogenization theory [18]. This method has turned topology optimization into a form of size optimization and reduced its complexity to some extent. A commonly used approach for representing materials in topology optimization problems is artificial material modeling [44, 45], which is employed in this paper. In this methodology, the distribution of materials across the domain is defined based on the density of individual elements. By utilizing this model, it becomes possible to derive the mechanical characteristics of materials without the need to solve homogenization equations. Moreover, this model enables the generation of suitable topologies with reduced computational expenses compared to homogenization-driven models [46].

In artificial material model when IGA is used, the material density is considered as a continuous function in the design domain. If we consider this function with  $0 \leq \Phi(x) \leq 1$ , we can define it at any point as follows:

$$\Phi(x) = \begin{cases} 1 & \text{material} \\ 0 & \text{no material} \end{cases} \quad (19)$$

For isotropic materials, the density and material matrix at any point are expressed respectively as:

$$\rho(x) = \Phi(x)\rho^0, \quad (20)$$

$$\mathbf{D}(x) = \Phi(x)\mathbf{D}^0, \quad (21)$$

where  $\rho^0$  and  $\mathbf{D}^0$  are the density and material matrix of solid homogenous material, respectively.

Applying this formulation may lead to a solution with many intermediate densities i.e., gray areas. This issue is not desirable from the engineering point of view. To address this problem, Bendsøe [19] proposed the idea of a penalty exponent. By applying this coefficient, (21) can be rewritten as:

$$\mathbf{D}(x) = \Phi^\mu(x)\mathbf{D}^0. \quad (22)$$

This model is referred to as SIMP in the literature. Using this scheme, elements with intermediate density produce small stiffness relative to their volume. Experience shows that by choosing a sufficiently large  $\mu$  ( $\mu \geq 3$ ), the optimization results in 0–1 solution [20].

In element-based methods, the density in each finite element ( $\Phi^e$ ) is constant and is considered as design variable in optimization problem. In the method presented in this article, which is based on IGA, density function

is considered as a continuous function over the design domain and is approximated by using the NURBS basis functions as:

$$\Phi(r, s) = \sum_{i=0}^{n_p} \sum_{j=0}^{n_q} R_{i,j}^{p,q}(r, s)\Phi_{ij}, \quad (23)$$

where  $\Phi_{ij}$  are the values of density function in control points and can be considered as design variables in topology optimization problem. The stiffness matrix (11), can now be rewritten as:

$$\mathbf{k} = \int \bar{\mathbf{B}}^T \Phi^\mu \bar{\mathbf{D}}^0 \bar{\mathbf{B}} dx dy dz, \quad (24)$$

where  $\bar{\mathbf{D}}^0$  represents material elasticity matrix of the solid part in local coordinate system.

### 4 Optimization procedure

The optimization problem considered in this article is the minimization of mean compliance, which is a common problem in structural topology optimization. This problem is expressed as minimizing the total elastic strain energy of the structure while applying a volume constraint. The general form of this problem can be expressed as:

$$\begin{aligned} \min c(x_i) \\ V(x_i) \leq V^{\max} \\ x_i^{\min} \leq x_i \leq x_i^{\max}, \quad i = 1, \dots, n \end{aligned} \quad (25)$$

where  $c$  is the total elastic strain energy,  $V$  is the volume of structure, and  $V^{\max}$  is the upper limit of the volume constraint.  $x_i$  represent the design variables which are limited between two values of  $x_i^{\min}$  and  $x_i^{\max}$  as lower and upper limits, respectively.

According to the previous section, values of densities at the control points  $\Phi_{ij}$  are considered as design variables which are limited between zero and one. In practice, to prevent numerical problems and singularities in the analysis model, a very small value is assigned to the lower limit of the density. Denoting  $\Phi^{\min}$  for this value, the optimization problem of (25) can be reordered as:

$$\begin{aligned} V(\Phi_{ij}) \leq V^{\max} \\ 0 \leq \Phi^{\min} \leq \Phi_i \leq 1, \quad i = 1, \dots, n \end{aligned} \quad (26)$$

Note that number of design variables,  $n$ , is equal to the total number of control points, where can be simply find as:

$$n = (n_p + 1) + (n_q + 1). \quad (27)$$

The approach employed in this article involves implementing the control net refinement method during the optimization process. NURBS has the capability to refine the

control net through either knot insertion or increasing the degree of the function [21]. For the specific purpose of this study, the knot insertion technique is utilized. This method entails dividing knot spans into smaller ones by inserting new knots. The refined basis functions are derived by incorporating the refined nodal vectors in Eqs. (1) and (2). The refined control points are then obtained through a linear combination of the original control points.

Considering the one-dimensional b-spline function, by inserting knot  $\bar{r}$  where  $\bar{r} \in [r_k, r_{k+1}]$ , the new  $n + 1$  control points  $Q_i (i = 1, \dots, n + 1)$  are formed from the original control point  $P_i (i = 1, \dots, n)$  by:

$$Q_i = \alpha_i P_i + (1 - \alpha_i) P_{i-1}, \quad (28)$$

where

$$\alpha_i = \begin{cases} 1 & i \leq k - p \\ \frac{\bar{r} - r_i}{r_{p+1} - r_i} & k - p < i < k \\ 0 & k < i \end{cases} \quad (29)$$

While a coarse control mesh enables the designer to generate a smooth surface, refinement gives the opportunity to make a finer control net without changing the geometry. By performing this scheme, a model different from the geometric model is obtained for optimization process. In other words, we are dealing with two models here. First is a model with a coarser mesh and appropriate for shape modeling, which is called "geometric model" from now on. The second model, which we call the "analysis/optimization model", is a model with a finer mesh which is used for analysis and the TO process. These models for a typical shape are illustrated in Fig. 4. This allows the designer to choose the accuracy and computational cost required to perform analysis and topology optimization. Note that this issue is somewhat similar to the mesh generation in conventional finite elements, with the difference that, firstly, the geometric shape remains unchanged, and secondly, it does not impose a large computational cost. Finally, it should be noted that the geometric model is produced only once by the designer and the optimization algorithm uses that to construct the analysis/optimization model for optimization process.

MMA [47] is utilized for solving optimization problem. This algorithm which is based on mathematical programming produces an approximate sub-problem by using derivatives information of objective and constraint functions. The optimal solution of this sub-problem is considered as

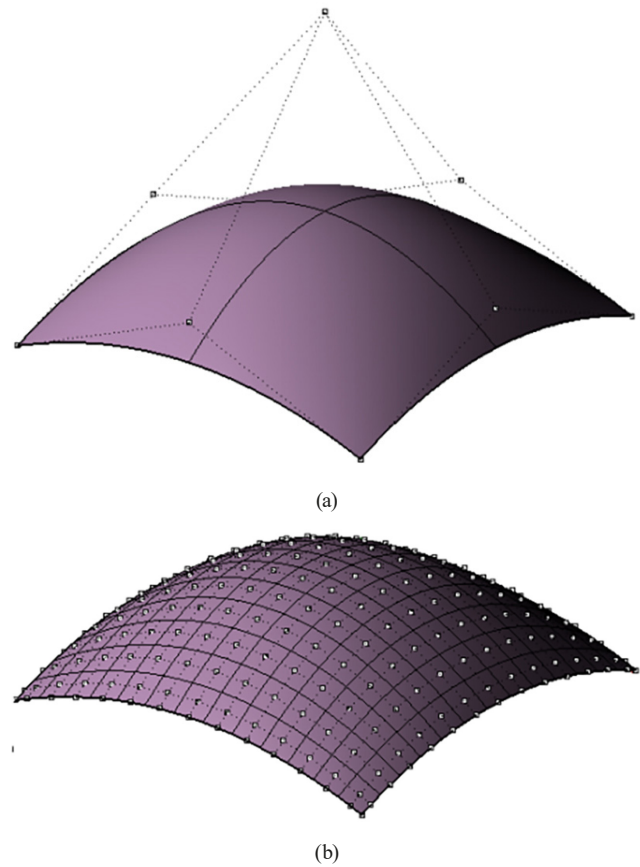


Fig. 4 Typical shapes of, (a) geometric and (b) analysis/optimization, models

the starting point in the next step of optimization, and this procedure continues until convergence is reached. In each optimization step, sensitivity analysis should be performed to obtain derivatives of the objective function and the volume constraint with respect to the design variables. This issue will be explained in the next section.

The optimization process introduced in this article can be shown as a flowchart in Fig. 5. As can be observed in this figure, after the construction of the geometric model, the analysis/optimization model is produced, and then, in each iteration, by performing analysis, sensitivity analysis and optimization, the design is improved until the global convergence.

### 5 Sensitivity analysis

Generally, there are three categories of sensitivity analysis methods: Analytical, numerical and semi-analytical methods. In analytical methods, the derivative values are obtained with explicit functions with respect to the design variables. In numerical methods, the derivatives of objective and constraints functions are obtained by using different numerical methods such as finite difference.

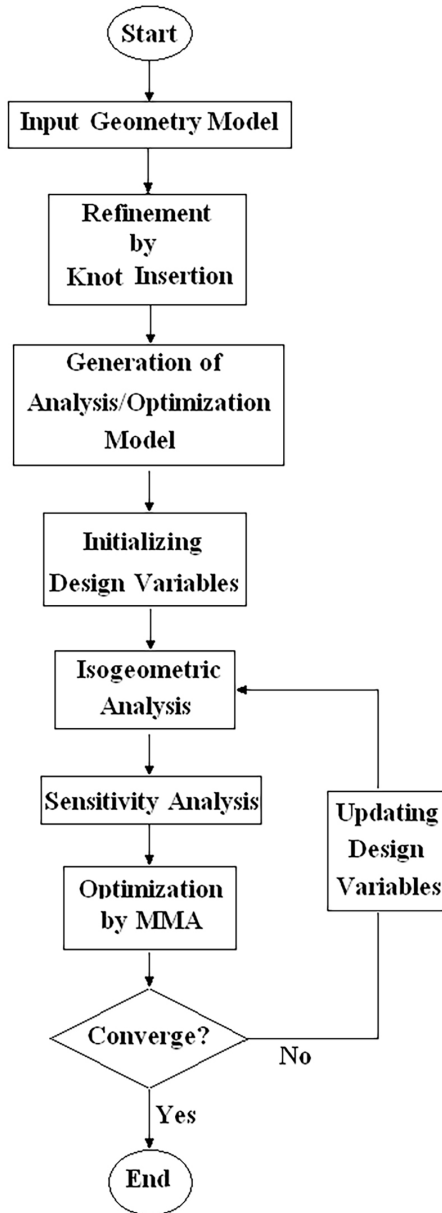


Fig. 5 The flowchart of optimization process

And finally, in semi-analytical methods, both analytical and numerical methods are applied. For a review on sensitivity analysis methods, the readers are referred to [48, 49]. In this paper, an analytical method is used.

The elastic strain energy can be expressed as:

$$c = \frac{1}{2} \mathbf{U}^T \mathbf{F} = \frac{1}{2} \mathbf{U}^T \mathbf{K} \mathbf{U}, \quad (30)$$

where  $\mathbf{U}$  and  $\mathbf{F}$ , respectively, are vectors of nodal displacements and loads and  $\mathbf{K}$  is the coefficient matrix of structure. Differentiating (30) and taking the advantage of symmetry of the stiffness matrix, derivatives of elastic strain energy with respect to design variables can be written as:

$$\frac{\partial c}{\partial x_i} = \frac{1}{2} \mathbf{U}^T \frac{\partial \mathbf{K}}{\partial x_i} \mathbf{U} + \mathbf{U}^T \mathbf{K} \frac{\partial \mathbf{U}}{\partial x_i}, \quad i = 1, \dots, n. \quad (31)$$

Differentiating equilibrium Eq. (32), and assuming that the loads are independent from the design variables, Eq. (33) is obtained:

$$\mathbf{K} \mathbf{U} = \mathbf{F}, \quad (32)$$

$$\mathbf{K} \frac{\partial \mathbf{U}}{\partial x_i} = -\frac{\partial \mathbf{K}}{\partial x_i} \mathbf{U}. \quad (33)$$

Substituting (33) to (31), the design sensitivity expression can be written as:

$$\frac{\partial c}{\partial x_i} = -\frac{1}{2} \mathbf{U}^T \frac{\partial \mathbf{K}}{\partial x_i} \mathbf{U}, \quad i = 1, \dots, n. \quad (34)$$

Eq. (34) demonstrates that the derivative of the strain energy with respect to a design variable depends on derivative of stiffness matrix. It should be pointed out that this relationship is regardless of the type of design variables. Considering that the stiffness matrix is an explicit function of the design variables  $\Phi_{ij}$  according to (23) and (24), its derivative with respect to the design variables can be easily obtained as:

$$\frac{\partial k}{\partial \Phi_{ij}} = \int \bar{\mathbf{B}}^T \mu \Phi^{\mu-1} \bar{\mathbf{D}}^0 \bar{\mathbf{B}} \, dx dy dz. \quad (35)$$

## 6 Numerical examples

In this section, some numerical examples are examined to demonstrate the capability and effectiveness of the implemented optimization method. In these examples, the optimal topology of the shell structure is found by using material distribution method introduced in this article, and the results are discussed. In all of the following examples, the values of modulus of elasticity and Poisson's ratio are considered as  $E = 1 \times 10^5$  and  $\nu = 0.3$  respectively. Shell thickness is equal to  $t = 0.1$  and the magnitude of point load is assumed to be  $p = 1$ . The volume fraction is taken as  $V/V^{\max} = 40\%$  in all the examples.

### 6.1 Example 1

A shell structure composed of four plane sheets is investigated as the first example. This structure is subjected to a concentrated load in the center and is clamped in its four corners by simple supports. The dimensions, loading and boundary conditions of the structure are illustrated in Fig. 6. Due to the symmetry condition, a quarter of the

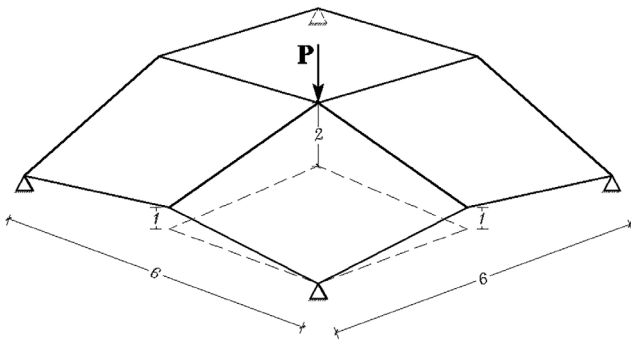


Fig. 6 The dimensions, loading and boundary conditions of example 1

entire structure can be modeled and solved by considering the appropriate support conditions. The exponent  $\mu = 5$  is used for penalizing the density function.

As mentioned earlier, in the optimization scheme proposed in this article, different models are used for geometry and analysis/optimization. In this example, a  $4 \times 4$  control net has been used for geometric modeling. Then, by refining the original model, a finer net of control points including 14 points in each direction, is created for analysis/optimization model. These models are shown in Figs. 7 (a) and (b), respectively. Degree of NURBS functions in both models is equal to 2. The condition of three orthogonal vectors at two arbitrary boundary points, together with symmetry boundary condition, is illustrated in Fig. 8.

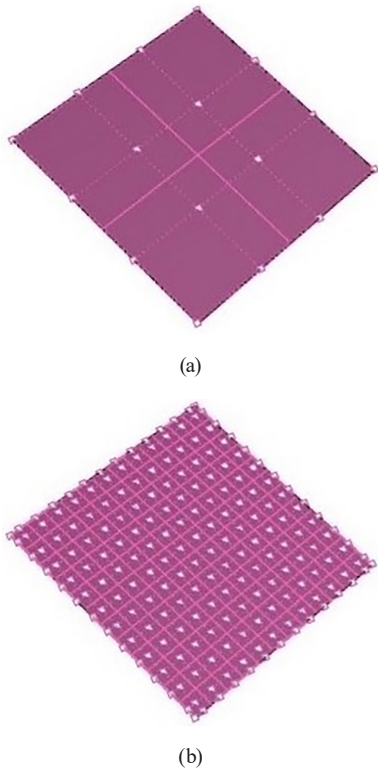


Fig. 7 Control net for example 1, (a) geometry and (b) analytical/optimization models

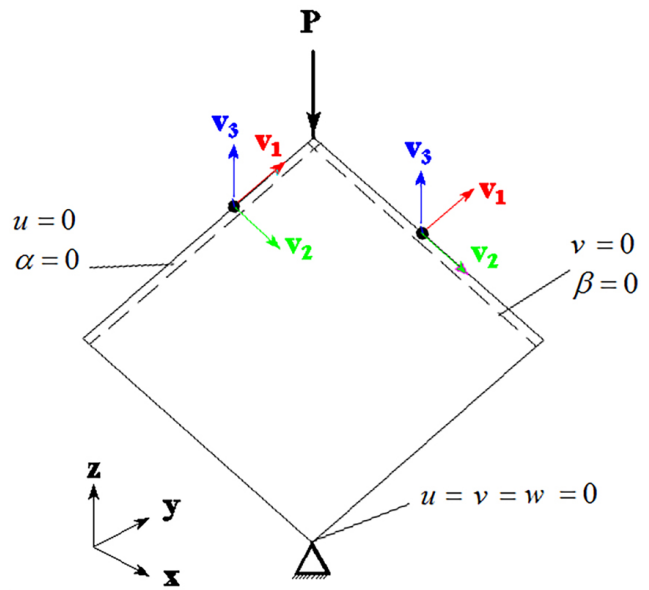


Fig. 8 Unit vectors and symmetry support condition of example 1

The optimal topology of this example is shown in Fig. 9. In this figure, the black regions indicate the presence of materials, while the white areas represent voids. The initial boundaries of the design domain are also shown in this figure, for a better 3D imagination.

The result shows that there are gray regions in the formed boundaries. These regions represent areas with intermediate density, i.e., values between zero and one. In the following, to investigate the effect of the mesh size, present example is solved with finer control nets. For this purpose, the initial net is refined into  $24 \times 24$ ,  $34 \times 34$  and  $44 \times 44$  analysis/optimization nets. The results of all meshes are shown in Fig. 10. As can be observed, the fineness of the control net, leads to similar results, but with fewer gray areas and sharper boundaries. It can be seen that in the proposed optimal design process, after geometric

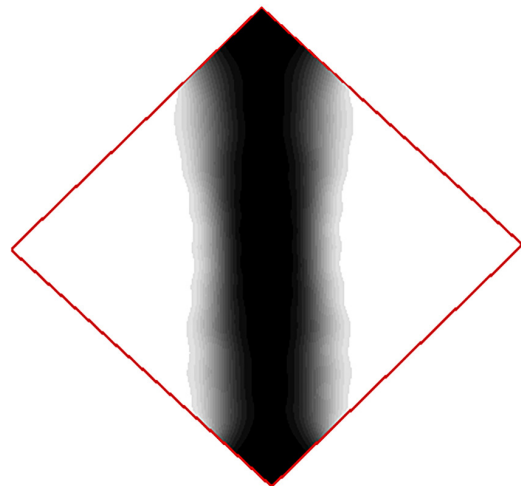
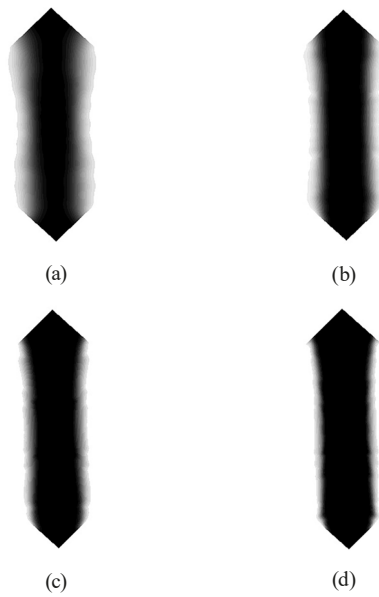


Fig. 9 Optimal solution of example 1



**Fig. 10** Results of example one with, (a)  $14 \times 14$ , (b)  $24 \times 24$ , (c)  $34 \times 34$  and (d)  $44 \times 44$ , analytical/optimization control nets

modeling, the designer can determine the dimensions of the appropriate analytical/optimization according to the computational cost and desired accuracy.

The whole structure is shown in Fig. 11 (a). The resulting optimal topology represents a truss-shaped structure that transmits forces to the supports by four members. Fig. 11 (b) illustrates the FEM based result [39]. It can be

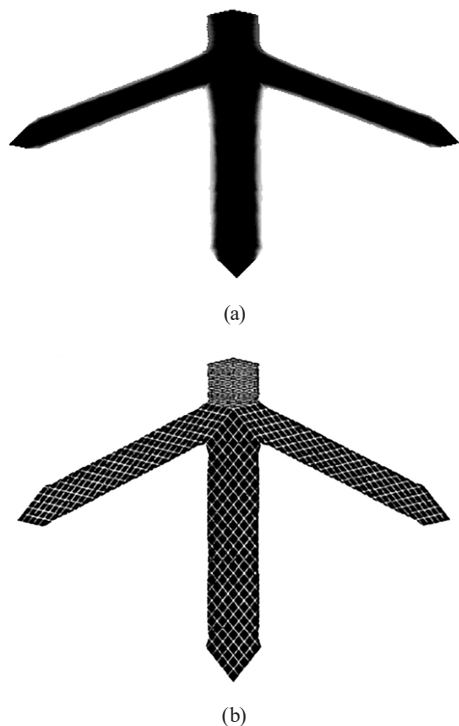


**Fig. 11** Final result of example one, (a) Complete optimal structure of example one, (b) Result of example one by using FEM based method [39]

seen that the outcomes of both methods are quite similar. Fig. 12 shows the variation of strain energy and total volume of the  $44 \times 44$  analytical/optimization mesh model, during optimization iterations. From this figure, it can be noted that the volume constraint may not always be satisfied in early iterations, resulting in fluctuations in the volume and strain energy diagrams. This phenomenon may arise from the nature of MMA, where sometimes relaxes constraints to achieve the desired solution. However after the initial steps, the constraint are satisfied, leading to a reduction in fluctuations and eventually disappearing of them. The graph shows decreasing trend of the strain energy as the objective function, along with its convergence at the end of the optimization process. Additionally, convergence of the total volume can be observed in this graph.

Having Eqs. (34–35), one analysis per optimization cycle is sufficient to generate the necessary derivative information. Based on the analysis framework outlined in sec. 2, each control point possesses 5 degrees of freedom. Consequently, the dimensions of the linear equation system required for  $14 \times 14$ ,  $24 \times 24$ ,  $34 \times 34$  and  $44 \times 44$  models will be  $70 \times 70$ ,  $120 \times 120$ ,  $170 \times 170$  and  $220 \times 220$ , respectively. Given the crucial importance of computational time in topology optimization, Table 1 outlines the CPU time devoted for optimization of each model. It should be noted that all modeling was performed on a computer equipped with Intel® Core™ i5-2450M CPU @ 2.50GHz. The devise is configured with 8.00 gigabytes of RAM.

### 6.2 Example 2

In this example, a cylindrical shell structure is investigated. This structure is a simple beam with a tubular cross-section,

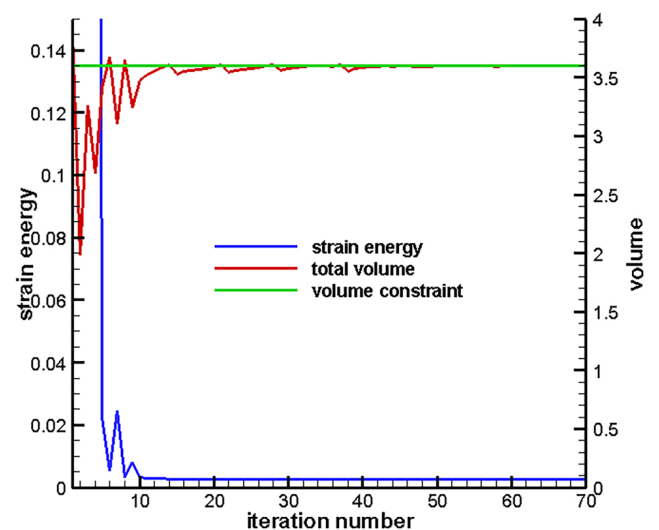


**Fig. 12** Variation of strain energy and total volume of example one

**Table 1** Computational cost of different models in example one

analytical/computational model	dimension of equation system	CPU time for the optimization process (second)
14 × 14	70 × 70	350
24 × 24	120 × 120	1190
34 × 34	170 × 170	2450
44 × 44	220 × 220	4480

having a length of 16 and a diameter of 4, which is subjected to a concentrated load in its mid-span as shown in Fig. 13 (a). Similar to first example, due to symmetry, a quarter of the problem is modeled and solved by applying appropriate support conditions (Fig. 13 (a)). A 6 × 6 control net is used for geometric modeling (Fig. 13 (b)). Degree of NURBS functions and penalty coefficient are equal to 2 and 5, respectively. Analytical/optimization models with 14 × 14, 26 × 26, 34 × 34 and 50 × 50 control nets are used for optimization. Fig. 14 shows the results of each case along with final values of strain energies. It is observed that for the finer nets, the values of strain energy increase due

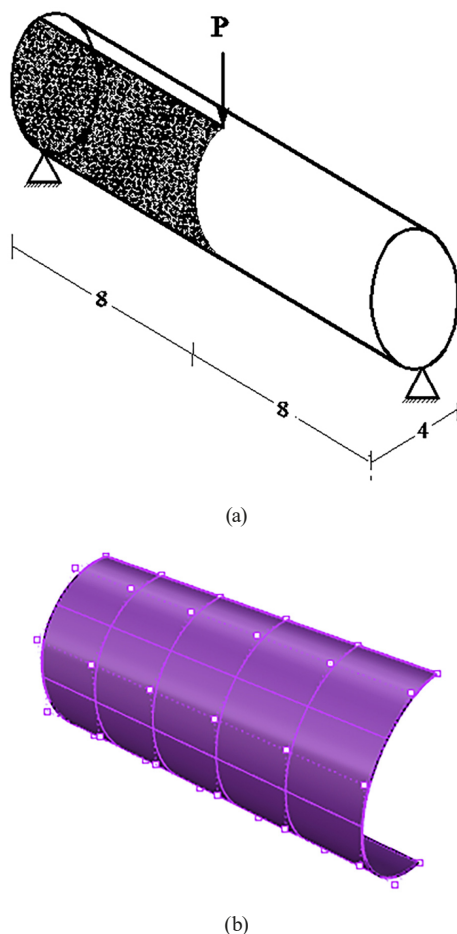


**Fig. 13** The structure of example 2, (a) initial domain and (b) geometric model

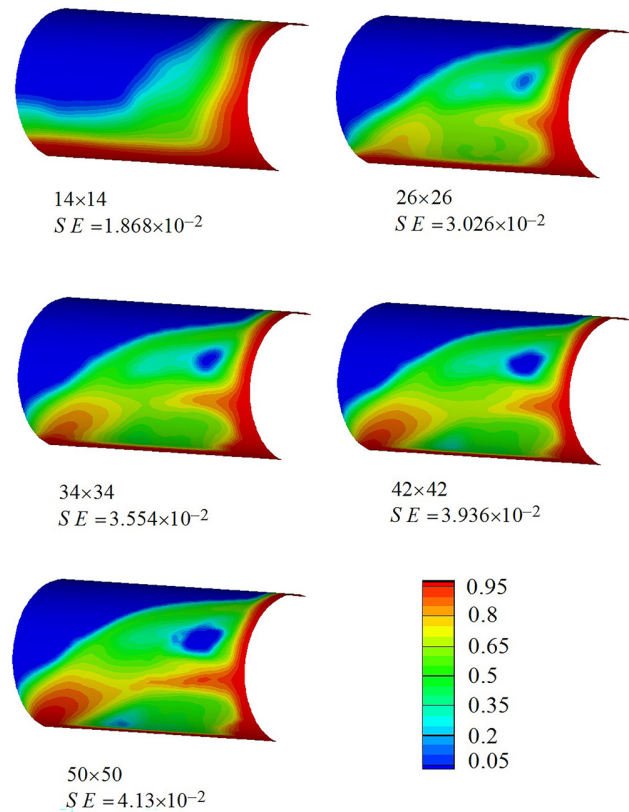


**Fig. 14** The results of example two, density contour together with final strain energy (SE) for various analytical/optimization control mesh, for  $\mu = 5$

to increase of degrees of freedom. It is obvious that finer meshes lead to more accurate results. In this figure, for better visualization, a colored contour is used to show the state of material distribution. The results show many areas with intermediate density values. It can also be seen that increasing the number of control points did not resolve this issue as the problem persists in models with finer control grids. Although a hole forms in the domain as the grid becomes finer, regions with intermediate density values prevent forming clear topology. Convergence of the solution indicates that the optimization process is completed correctly (Fig. 15). But as mentioned before, the answer with intermediate density is not applicable from a practical point of view.

In the next step, penalty exponent  $\mu$  is used to remove the intermediate density areas in SIMP approach. Fig. 16 shows the results of this example for  $\mu = 7$ . The results of this figure show that compared to the previous case ( $\mu = 5$ ), holes with relatively more clear boundaries have been created and topology of structure has been determined to some extent, but still areas with intermediate density (green color) are observed even in the fine nets. Finally, the present example is solved with  $\mu = 9$ . The results of this case can be observed in Fig. 17. In all nets, the green areas with intermediate density values are much lower than the previous two cases.

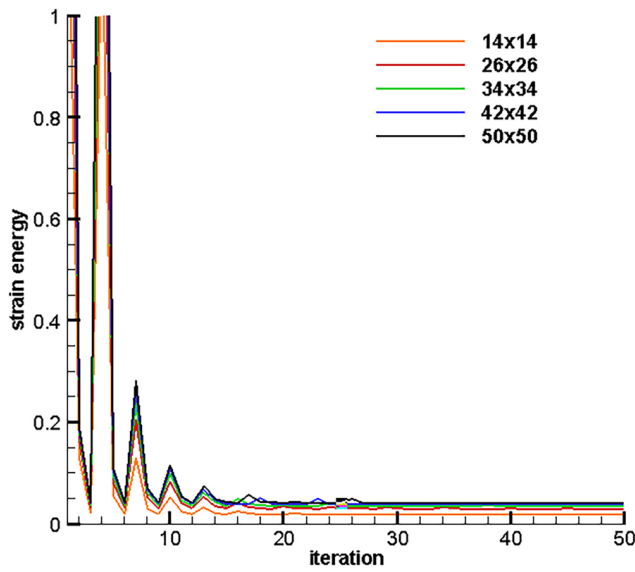


Fig. 15 Iteration history of example two

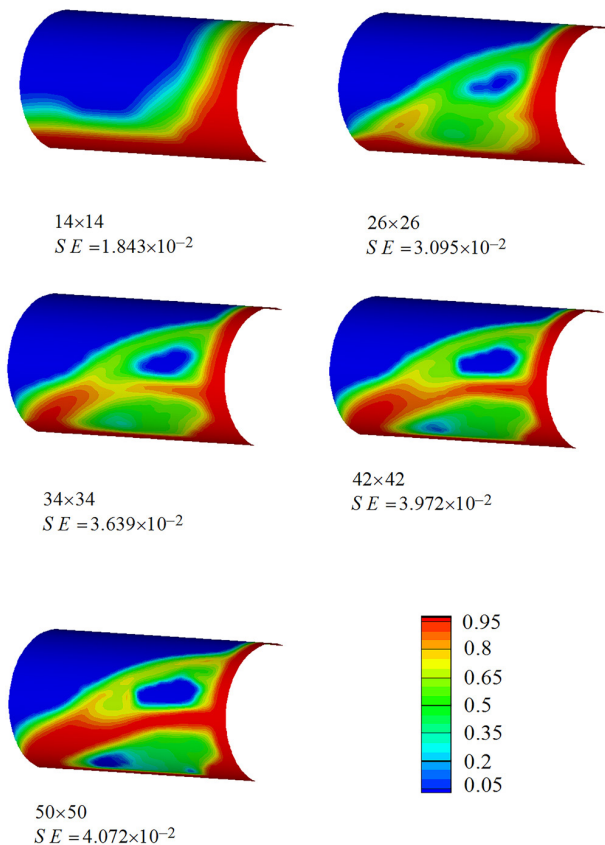


Fig. 16 The results of example two, density contour together with final strain energy (SE) for various analytical/optimization control mesh, for  $\mu = 7$

It can also be seen that the extent of green area is reduced in finer control nets, and finally in the  $50 \times 50$  net, final boundaries are clearly visible and the optimal topology is reached. It can be seen that by choosing penalty factor  $\mu = 9$ , except for the  $14 \times 14$  net, which is a coarse mesh, the final

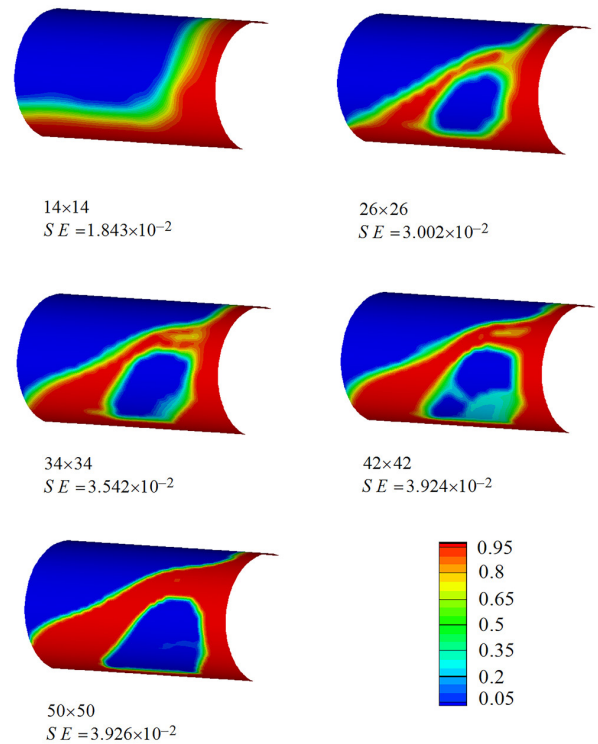


Fig. 17 The results of example two, density contour together with final strain energy (SE) for various analytical/optimization control mesh, for  $\mu = 9$

topologies are similar. Fig. 18 shows the result of topology optimization for the complete structure with applied load and support conditions in different views.

Results of this example show that value of penalty coefficient of material distribution function is essential for finding the optimal and practical answer. As mentioned

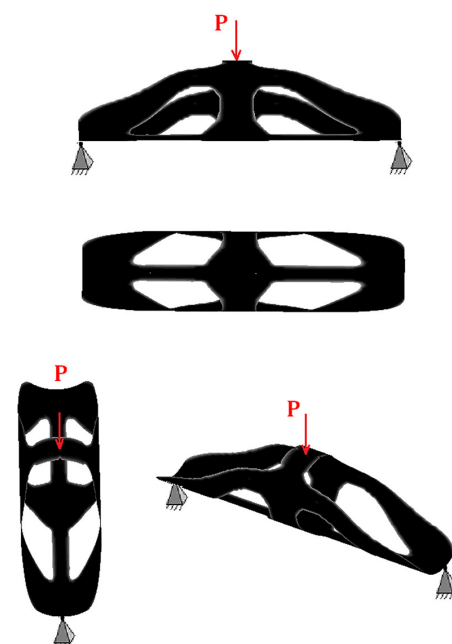


Fig. 18 Final complete optimal topology of example two

earlier in Section 3, values greater than 3 have been proposed for this coefficient. In this example, it was observed that the value of 9 with an appropriate mesh led to a correct optimal answer with clear boundaries.

### 6.3 Example 3

Topology optimization of a freeform shell structure is considered as the final example of this article. The initial design domain of this structure, shown in Fig. 19, is a box with curved edges and a hole in its top center. A linear distributed load is applied around the hole and it is restrained at the four midpoints of the bottom edges by simple supports. Due to its symmetry, one quarter of the structure is modeled. The purpose of this example is to investigate the effect of NURBS degree and the penalty coefficient value on the final optimal results. To solve this example, first, degree of NURBS basis function is considered equal to  $p = 2$  and the analytical/optimization model is formed with a  $44 \times 44$  control mesh. The problem is solved with the penalty coefficient with different values of 3, 5, 7 and 9. Contour of obtained results is shown in Fig. 20. By increasing the values of  $\mu$ , areas with intermediate density decrease. For the values 3 and 5, the results are not satisfactory, and by increasing the penalty factor to 7 and 9, acceptable results are obtained. It can be seen that the results of the last two cases have a slight difference in the boundaries and strain energy values.

Next, to check the effect of the NURBS degree, this example is modeled and solved with  $p = 3$  and a  $45 \times 45$  mesh. The results are presented in Fig. 21. It can be observed that the results are very similar to the previous case. For the  $\mu$  values of 3 and 5, the results are unacceptable, whereas they are reasonable for the values of 7 and 9. It can also be concluded that the degree of the NURBS has no effect on the optimal topology. It is obvious that the difference in the strain energy values is due to the difference in the degree of the NURBS basis function and

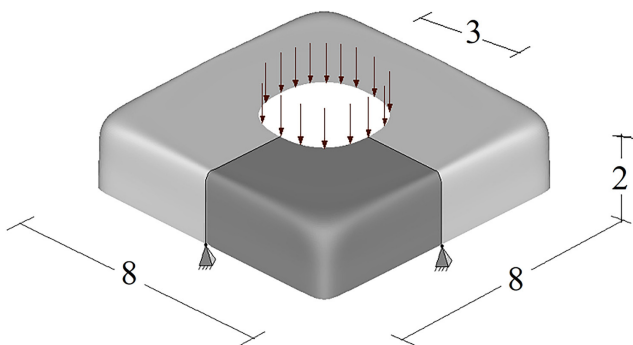


Fig. 19 The problem description of example three

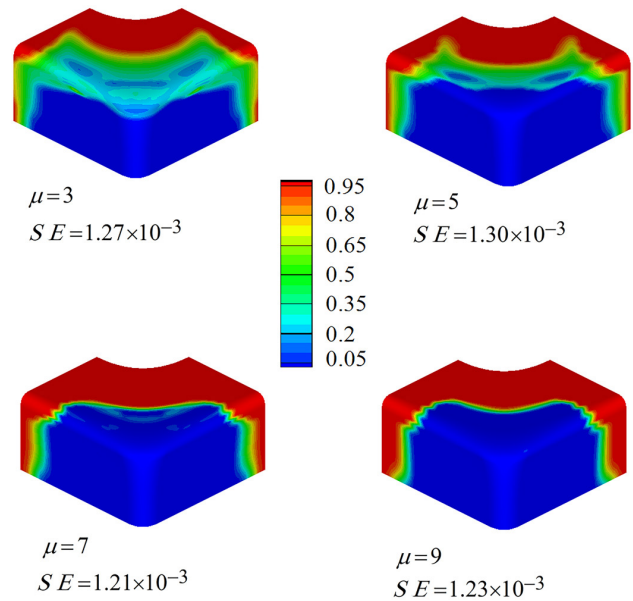


Fig. 20 Results of example three, density contour together with final strain energy (SE) for various  $\mu$  ( $p = 2, 44 \times 44$  mesh)

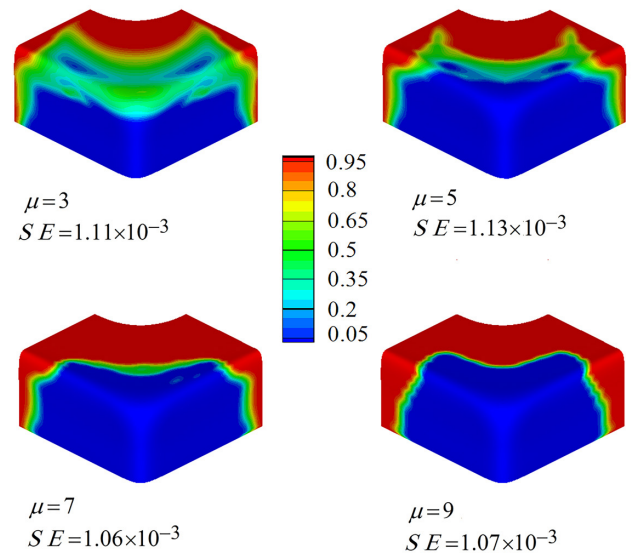


Fig. 21 Results of example three, density contour together with final strain energy (SE) for various  $\mu$  ( $p = 3, 45 \times 45$  mesh)

accuracy of the two models. The optimal topology of complete structure for  $p = 3$  and  $\mu = 9$  is shown in Fig. 22. It is evident that the results remain constant when using various NURBS degrees, indicating that the solution is not influenced by the degree of the polynomial employed.

### 7 Conclusions

In this article, an SIMP based method, along with isogeometric analysis, is employed for topology optimization of shell structures. NURBS basis functions have been used for approximation of density function of artificial materials. The geometry is initially created using a coarse mesh of



Fig. 22 Optimal topology of example three

control points, which is then refined to achieve the desired accuracy in the optimization and analysis model. The density function is approximated using NURBS at the control points, treating their values as design variables in the optimization problem. The optimal material distribution in the design domain is determined by minimizing the strain energy with a volume constraint. Sensitivity analysis is conducted and the problem is solved by using MMA. The results indicate convergence of objective and constraint functions to the

## References

- [1] Maxwell, J. C. "On reciprocal figures, frames and diagrams of forces", *Transactions of the Royal Society of Edinburgh*, 26(1), pp. 1–40, 1870.  
<https://doi.org/10.1017/S0080456800026351>
- [2] Hajela, P., Lee E. "Genetic algorithms in truss topological optimization", *International Journal of Solids and Structures*, 32(22), pp. 3341–3357, 1995. [online] Available at: <https://www.sciencedirect.com/science/article/abs/pii/002076839400306H> [Accessed: 10 November 2024]
- [3] Kaveh, A., Kalatjari V. "Topology optimization of trusses using genetic algorithm, force method and graph theory", *International Journal for Numerical Methods in Engineering*, 58(5), pp. 771–791, 2003. [online] Available at: <https://onlinelibrary.wiley.com/doi/abs/10.1002/nme.800> [Accessed: 10 November 2024]
- [4] Kaveh, A., Zolghadr, A. "Topology optimization of trusses considering static and dynamic constraints using the CSS", *Applied Soft Computing*, 13(5), pp. 2727–2734, 2013.  
<https://doi.org/10.1016/j.asoc.2012.11.014>
- [5] Kaveh, A., Ahmadi, B. "Sizing, geometry and topology optimization of trusses using force method and supervised charged system search", *Structural Engineering and Mechanics*, 50(3), pp. 365–382, 2014.  
<http://doi.org/10.12989/sem.2014.50.3.365>
- [6] Habashneh, M., Rad, M. M. "Plastic-limit probabilistic structural topology optimization of steel beams", *Applied Mathematical Modelling*, 128, pp. 347–369, 2024.  
<https://doi.org/10.1016/j.apm.2024.01.029>
- [7] Kaveh, A. Talatahari, S. "Optimal design of skeletal structures via the charged system search algorithm", *Structural and Multidisciplinary Optimization*, 41, pp. 893–911, 2010.  
<https://doi.org/10.1007/s00158-009-0462-5>
- [8] Merczel, D. B., Somja, H., Aribert, J. M., Lógó, J. "On the behaviour of concentrically braced frames subjected to seismic loading", *Periodica Polytechnica Civil Engineering*, 57(2), pp. 113–122, 2013. [online] Available at: <https://pp.bme.hu/ci/article/view/7167> [Accessed: 10 November 2024]
- [9] Bruggi, M., Milani, G., Taliercio, A. "Design of the optimal fiber-reinforcement for masonry structures via topology optimization", *International Journal of Solids and Structures*, 50(13), pp. 2087–2106, 2013.  
<https://doi.org/10.1016/j.ijsolstr.2013.03.007>
- [10] Zakian, P., Kaveh, A. "Topology optimization of shear wall structures under seismic loading", *Earthquake Engineering and Engineering Vibration*, 19, pp. 105–116, 2020.  
<https://doi.org/10.1007/s11803-020-0550-5>
- [11] Maute, K., Ramm, E. "Adaptive topology optimization of shell structures", *AIAA Journal*, 35(11), pp. 1767–1773, 1997.  
<https://doi.org/10.2514/2.25>
- [12] Hassani, B., Tavakkoli, S. M., Ghasemnejad, H. "Simultaneous shape and topology optimization of shell structures", *Structural and Multidisciplinary Optimization*, 48, pp. 221–233, 2013.  
<https://doi.org/10.1007/s00158-013-0894-9>

final values, demonstrating the stability of the solution. It was observed that finer control nets produce more clear boundaries and better results. The penalty exponent plays a crucial role in achieving an acceptable solution, often requiring higher values. In some examples, high values of  $\mu$  (e.g., 9) are needed to reach a suitable solution. The impact of NURBS degree on the optimal topology is found to be negligible.

Results indicate that mesh sensitivity plays a crucial role in finding the optimal topology for the examples of this article. Control mesh should be fine enough in analytical/optimization model to get desired solution with minimum gray area. As future research, other TO methods such as the level set approach, can be employed to solve this issue. Furthermore, based on the presented formulation for shape modeling, incorporating shape and topology optimization for a simultaneous optimization problem is straightforward.

## Acknowledgement

The authors wish to express their gratitude to Professor Krister Svanberge for providing the MMA code.

- [13] Fu, J., Li, H., Gao, L., Xiao, M. "Design of shell-infill structures by a multiscale level set topology optimization method", *Computers & Structures*, 212, pp. 162–172, 2019.  
<https://doi.org/10.1016/j.compstruc.2018.10.006>
- [14] Rad, M. M., Habashneh, M., Lógó, J., "Reliability based bi-directional evolutionary topology optimization of geometric and material nonlinear analysis with imperfections", *Computers & Structures*, 287, 107120, 2023.  
<https://doi.org/10.1016/j.compstruc.2023.107120>
- [15] Habashneh, M., Rad, M. M. "Optimizing structural topology design through consideration of fatigue crack propagation", *Computer Methods in Applied Mechanics and Engineering*, 419, 116629, 2024.  
<https://doi.org/10.1016/j.cma.2023.116629>
- [16] Habashneh, M., Cucuzza, R., Domaneschi, M., Rad, M. M. "Advanced elasto-plastic topology optimization of steel beams under elevated temperatures", *Advances in Engineering Software*, 190, 103596, 2024.  
<https://doi.org/10.1016/j.advengsoft.2024.103596>
- [17] Lógó, J., Ismail, H. "Milestones in the 150-year history of topology optimization: A review", *Computer Assisted Methods in Engineering and Science*, 27(2–3), pp. 97–132, 2020.
- [18] Bendsoe, M. P., Kikuchi, N. "Generating optimal topologies in structural design using a homogenization method", *Computer Methods in Applied Mechanics and Engineering*, 71(2), pp. 197–224, 1988.  
[https://doi.org/10.1016/0045-7825\(88\)90086-2](https://doi.org/10.1016/0045-7825(88)90086-2)
- [19] Bendsoe, M. P. "Optimal shape design as a material distribution problem", *Structural Optimization*, 1, pp. 193–202, 1989.  
<https://doi.org/10.1007/BF01650949>
- [20] Bendsoe, M. P., Sigmund, O. "Topology optimization: Theory, methods, and applications", Springer Science & Business Media, 2002. ISBN 978-3-540-42992-0
- [21] Hughes, T. J. R., Cottrell, J. A., Bazilevs, Y. "Isogeometric analysis: CAD, finite elements, NURBS, exact geometry and mesh refinement", *Computer Methods in Applied Mechanics and Engineering*, 194(39–41), pp. 4135–4195, 2005.  
<https://doi.org/10.1016/j.cma.2004.10.008>
- [22] Gao, J., Xiao, M., Zhang, Y., Gao, L. "A comprehensive review of isogeometric topology optimization: methods, applications and prospects", *Chinese Journal of Mechanical Engineering*, 33(1), pp. 1–14, 2020.  
<https://doi.org/10.1186/s10033-020-00503-w>
- [23] Hassani, B., Khanzadi, M., Tavakkoli, S. M. "An isogeometrical approach to structural topology optimization by optimality criteria", *Structural and Multidisciplinary Optimization*, 45, pp. 223–233, 2012.  
<https://doi.org/10.1007/s00158-011-0680-5>
- [24] Tavakkoli, S. M., Hassani, B., Ghasemnejad, H. "Isogeometric topology optimization of structures by using MMA", *International Journal of Optimization in Civil Engineering*, 3(2), pp. 313–326, 2013.
- [25] Gao, J., Gao, L., Luo, Z., Li, P. "Isogeometric topology optimization for continuum structures using density distribution function", *International Journal for Numerical Methods in Engineering*, 119(10), pp. 991–1017, 2019.  
<https://doi.org/10.1002/nme.6081>
- [26] Ghasemi, H., Park, H. S., Rabczuk, T. "A level-set based IGA formulation for topology optimization of flexoelectric materials", *Computer Methods in Applied Mechanics and Engineering*, 313, pp. 239–258, 2017.  
<https://doi.org/10.1016/j.cma.2016.09.029>
- [27] Jahangiry, H. A., Tavakkoli, S. M. "An isogeometrical approach to structural level set topology optimization", *Computer Methods in Applied Mechanics and Engineering*, 319, pp. 240–257, 2017.  
<https://doi.org/10.1016/j.cma.2017.02.005>
- [28] Xu, M., Wang, S., Xie, X. "Level set-based isogeometric topology optimization for maximizing fundamental eigenfrequency", *Frontiers of Mechanical Engineering*, 14(2), pp. 222–234, 2019.  
<https://doi.org/10.1007/s11465-019-0534-1>
- [29] Zhang, W., Yuan, J., Zhang, J., Guo, X. "A new topology optimization approach based on Moving Morphable Components (MMC) and the ersatz material model", *Structural and Multidisciplinary Optimization*, 53, pp. 1243–1260, 2016.  
<https://doi.org/10.1007/s00158-015-1372-3>
- [30] Xie, X., Wang, S., Xu, M., Wang, Y. "A new isogeometric topology optimization using moving morphable components based on R-functions and collocation schemes", *Computer Methods in Applied Mechanics and Engineering*, 339, pp. 61–90, 2018.  
<https://doi.org/10.1016/j.cma.2018.04.048>
- [31] Xie, X., Wang, S., Xu, M., Jiang, N., Wang, Y. "A hierarchical spline based isogeometric topology optimization using moving morphable components", *Computer Methods in Applied Mechanics and Engineering*, 360, 112696, 2020.  
<https://doi.org/10.1016/j.cma.2019.112696>
- [32] Stegmann, J., Lund E. "Nonlinear topology optimization of layered shell structures", *Structural and Multidisciplinary Optimization*, 29, pp. 349–360, 2005.  
<https://doi.org/10.1007/s00158-004-0468-y>
- [33] Park, K.-S., Youn, S.-K. "Topology optimization of shell structures using adaptive inner-front (AIF) level set method", *Structural and Multidisciplinary Optimization*, 36, pp. 43–58, 2008.  
<https://doi.org/10.1007/s00158-007-0169-4>
- [34] Lund, E. "Buckling topology optimization of laminated multi-material composite shell structures", *Composite Structures*, 91(2), pp. 158–167, 2009.  
<https://doi.org/10.1016/j.compstruct.2009.04.046>
- [35] Clausen, A., Andreassen, E., Sigmund, O. "Topology optimization of 3D shell structures with porous infill", *Acta Mechanica Sinica*, 33(4), pp. 778–791, 2017.  
<https://doi.org/10.1007/s10409-017-0679-2>
- [36] Townsend, S., Kim, H. A. "A level set topology optimization method for the buckling of shell structures", *Structural and Multidisciplinary Optimization*, 60, pp. 1783–1800, 2019.  
<https://doi.org/10.1007/s00158-019-02374-9>
- [37] Ansola, R., Canales, J., Tárrago, J. A., Rasmussen, J. "An integrated approach for shape and topology optimization of shell structures", *Computers & Structures*, 80(5–6), pp. 449–458, 2002.  
[https://doi.org/10.1016/S0045-7949\(02\)00019-6](https://doi.org/10.1016/S0045-7949(02)00019-6)

- [38] Ansola, R., Canales, J., Tarrago, J. A., Rasmussen, J. "Combined shape and reinforcement layout optimization of shell structures", *Structural and Multidisciplinary Optimization*, 27, pp. 219–227, 2004.  
<https://doi.org/10.1007/s00158-004-0399-7>
- [39] Ansola, R., Canales, J., Tarrago, J. A., Rasmussen, J., "On simultaneous shape and material layout optimization of shell structures", *Structural and Multidisciplinary Optimization*, 24, pp. 175–184, 2002.  
<https://doi.org/10.1007/s00158-002-0227-x>
- [40] Meng, X., Xiong, Y., Xie, Y. M., Sun, Y., Zhao, Z.-L. "Shape–thickness–topology coupled optimization of free-form shells", *Automation in Construction*, 142, 104476, 2022.  
<https://doi.org/10.1016/j.autcon.2022.104476>
- [41] Zienkiewicz, O. C., Taylor, R. L. "El método de los elementos finitos" (The finite element method: solid mechanics (Vol. 2), Butterworth-Heinemann, 1995, ISBN 8448117603 (in Spanish)
- [42] Reissner, E. "The effect of transverse shear deformation on the bending of elastic plates", *Journal of Applied Mechanics*, 12(2), pp. 69–77, 1945.  
<https://doi.org/10.1115/1.4009435>
- [43] Uhm, T.-K., Youn, S.-K. "T-spline finite element method for the analysis of shell structures", *International Journal for Numerical Methods in Engineering*, 80(4), pp. 507–536, 2009.  
<https://doi.org/10.1002/nme.2648>
- [44] Zhou, M., Rozvany, G. I. N. "The COC algorithm, Part II: Topological, geometrical and generalized shape optimization", *Computer Methods in Applied Mechanics and Engineering*, 89(1–3), pp. 309–336, 1991.  
[https://doi.org/10.1016/0045-7825\(91\)90046-9](https://doi.org/10.1016/0045-7825(91)90046-9)
- [45] Bendsøe, M. P. Sigmund, O. "Material interpolation schemes in topology optimization", *Archive of Applied Mechanics*, 69, pp. 635–654, 1999.  
<https://doi.org/10.1007/s004190050248>
- [46] Rozvany, G. I. N. "A critical review of established methods of structural topology optimization", *Structural and Multidisciplinary Optimization*, 37, pp. 217–237, 2009.  
<https://doi.org/10.1007/s00158-007-0217-0>
- [47] Svanberg, K. "The method of moving asymptotes – a new method for structural optimization", *International Journal for Numerical Methods in Engineering*, 24(2), pp. 359–373, 1987.
- [48] Newman III, J. C., Taylor III, A. C., Barnwell, R. W., Newman, P. A., Hou, G. J. W. "Overview of sensitivity analysis and shape optimization for complex aerodynamic configurations", *Journal of Aircraft*, 36(1), pp. 87–96, 1999.  
<https://doi.org/10.2514/2.2416>
- [49] Van Keulen, F., Haftka, R. T., Kim, N. H. "Review of options for structural design sensitivity analysis. Part I: Linear systems", *Computer Methods in Applied Mechanics and Engineering*, 194(30–33), pp. 3213–3243, 2005.  
<https://doi.org/10.1016/j.cma.2005.02.002>